

## Supporting Information

### **In vivo-Stoffwechselbildung mit [1-<sup>13</sup>C]Pyruvat-d<sub>3</sub>, hyperpolarisiert durch reversiblen Austausch mit Parawasserstoff**

*H. de Maissin, P. R. Groß, O. Mohiuddin, M. Weigt, L. Nagel, M. Herzog, Z. Wang,  
R. Willing, W. Reichardt, M. Pichotka, L. Heß, T. Reinheckel, H. J. Jessen, R. Zeiser, M. Bock,  
D. von Elverfeldt, M. Zaitsev, S. Korchak, S. Glöggler, J.-B. Hövener, E. Y. Chekmenev,  
F. Schilling, S. Knecht\*, A. B. Schmidt\**

Supporting Information  
©Wiley-VCH 2021  
69451 Weinheim, Germany

## In Vivo Metabolic Imaging of [1-<sup>13</sup>C]Pyruvate-d<sub>3</sub> Hyperpolarized By Reversible Exchange With Parahydrogen

Henri de Maissin,<sup>‡</sup> Philipp R. Groß,<sup>‡</sup> Obaid Mohiuddin,<sup>‡</sup> Moritz Weigt,<sup>‡</sup> Luca Nagel, Marvin Herzog, Zirun Wang, Robert Willing, Wilfried Reichardt, Martin Pichotka, Lisa Heß, Thomas Reinheckel, Henning J. Jessen, Robert Zeiser, Michael Bock, Dominik von Elverfeldt, Maxim Zaitsev, Sergey Korchak, Stefan Glöggler, Jan-Bernd Hövener, Eduard Y. Chekmenev, Franz Schilling, Stephan Knecht,\* Andreas B. Schmidt\*

**Abstract:** Metabolic magnetic resonance imaging (MRI) using hyperpolarized (HP) pyruvate has shown promise as a non-invasive technique for diagnosing, staging, and monitoring response to treatment in cancer and other diseases. The clinically established method for producing HP pyruvate is dissolution dynamic nuclear polarization; however, it is rather expensive and slow. Here, we demonstrate fast (6 min), low-cost production of HP [1-<sup>13</sup>C]pyruvate-d<sub>3</sub> in aqueous solution using Signal Amplification By Reversible Exchange (SABRE), and *in vivo* metabolic MRI. The injected solution was sterile, non-toxic, pH neutral and contained ≈30 mM [1-<sup>13</sup>C]pyruvate-d<sub>3</sub> polarized to ≈11% (residual 250 mM methanol and 20 μM catalyst). It was obtained by rapid solvent evaporation and metal filtering. The procedure was well tolerated by all four mice studied here. This achievement is a significant step of making HP MRI available to a wider community. Fast, low-cost, and high-throughput parahydrogen-hyperpolarization has become a viable alternative for metabolic MRI of living organisms.

DOI: 10.1002/anie.202306654

## SUPPORTING INFORMATION

## Table of Contents

<b>EXPERIMENTAL PROCEDURES .....</b>	<b>2</b>
SAMPLE PREPARATION .....	2
EXPERIMENTAL SETUP .....	3
HYPERPOLARIZATION EXPERIMENTS .....	4
PURIFICATION .....	5
CONCENTRATION DETERMINATION .....	6
POLARIZATION CALCULATION .....	7
<i>In Vivo</i> EXPERIMENTS .....	7
<sup>1</sup> H MRI SEQUENCE AND PARAMETERS FOR ANATOMICAL REFERENCE:.....	7
<sup>13</sup> C CSI SEQUENCE AND PARAMETERS: .....	7
<sup>13</sup> C SELECTIVE bSSFP SEQUENCE AND PARAMETERS: .....	7
<sup>13</sup> C MRI DATA PROCESSING AND VISUALIZATION:.....	8
<b>ANALYSIS OF THE PURIFIED HYPERPOLARIZED SOLUTIONS.....</b>	<b>8</b>
CELL CULTURE AND MTT FOR CYTOTOXICITY .....	8
<b>MRI EXPERIMENTS.....</b>	<b>12</b>
<b>RELAXATION DATA USED TO DETERMINE <math>T_1</math> AND <math>T_{1\rho}</math> AT DIFFERENT MAGNETIC FIELDS.....</b>	<b>17</b>
<b>REMAINING METHANOL AND IRIIDIUM WITH RESPECT TO A POTENTIAL HUMAN TRANSLATION .....</b>	<b>18</b>
<b>REFERENCES USED IN SUPPORTING INFORMATION .....</b>	<b>19</b>
<b>AUTHOR CONTRIBUTIONS .....</b>	<b>19</b>

## Experimental Procedures

## Sample Preparation

The enrichment of parahydrogen (pH<sub>2</sub>) was conducted using a previously described setup and method,<sup>[1]</sup> yielding a pH<sub>2</sub> fraction of approximately 90% (Figure S1). Experimental samples were prepared, containing 50 mM sodium [1-<sup>13</sup>C]-pyruvate-d<sub>3</sub>, 6 mM IrIMes(COD)Cl pre-catalyst, 40 mM DMSO (Sigma Aldrich), and 1 mM ethylenediaminetetraacetic acid (EDTA disodium salt solution, 500 mM in H<sub>2</sub>O, CAS: 139-33-3) in methanol-d<sub>4</sub> (Sigma Aldrich, 99.8 atom % D). Following the mixing process, samples were subjected to 2-3 minutes of sonication. Subsequently the solutions were passed through a 1.2 µm syringe filter. The solutions were then degassed by introducing N<sub>2</sub> gas into the solution for approximately 1-2 minutes.

The synthesis of the IrIMes(COD)Cl pre-catalyst was accomplished using an established procedure.<sup>[2]</sup> Sodium [1-<sup>13</sup>C]-pyruvate-d<sub>3</sub> was formed by cautiously and gradually combining [1-<sup>13</sup>C]-pyruvic acid-d<sub>4</sub> (catalogue number 900845-SPEC, Sigma Aldrich, ≥99 atom % <sup>13</sup>C, ≥97 atom % D) with NaOD (sodium deuterioxide solution, 40 wt. % in D<sub>2</sub>O, CAS: 14014-06-3, Sigma, 99 atom % D). This reaction occurred in a D<sub>2</sub>O-filled flask that was placed in an ice water bath. Any remaining D<sub>2</sub>O was eliminated in a lyophilizer

## SUPPORTING INFORMATION

freeze dryer for moisture removal. Note however, that sodium [ $1\text{-}^{13}\text{C}$ ]-pyruvate- $\text{d}_3$  is also directly available from suppliers (e.g., Sigma Aldrich).

The phosphate buffered solutions (PBS) used for purification were prepared by dissolving a commercially available phosphate buffer powder (pH 7.3-7.5, 0.017 g/mL in water, high purity, SKU P7994-1EA, Sigma Aldrich) in either deionized  $\text{H}_2\text{O}$  or  $\text{D}_2\text{O}$  to obtain a PBS with neutral pH and osmolarity.

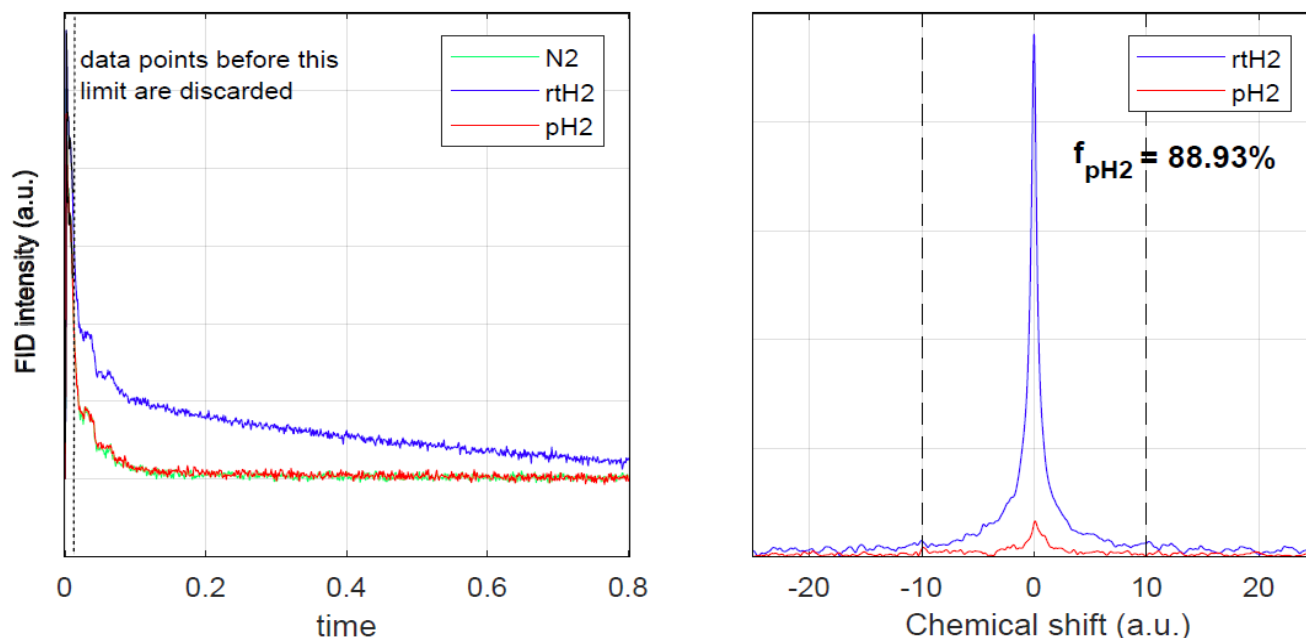


**Figure S1:** Time-domain and Fourier-transformed frequency-domain  $^1\text{H}$  NMR data of  $\text{N}_2$  gas (green; to subtract background signals), thermally equilibrated room temperature  $\text{H}_2$  gas (rtH $_2$ ; blue; 25 % pH $_2$ ) and pH $_2$ -enriched  $\text{H}_2$  gas (red) quantification. By comparing the signals of rtH $_2$  and pH $_2$ , which is NMR silent, the pH $_2$  enrichment of the latter was quantified to 88.93%. NMR was acquired using a 1T Benchtop NMR (Spinsolve Carbon 43, Magritek).

### Experimental Setup

A custom-built setup was developed for this study, incorporating a resistive solenoid coil (360mm length, 120mm inner diameter, two layers of 1.12mm copper wire, 47 compensation windings at each end of the solenoid) from an earlier experiment,<sup>[3]</sup> which produced a static magnetic field along the z-axis ( $B_0$ ). A saddle-shaped coil with one winding wrapped around a 320mm long, 100mm inner diameter tube generated a linearly polarized oscillating magnetic field along the x-axis ( $B_1$ ) for use in SLIC polarization transfer. The external laboratory magnetic field was shielded by a three-layer mu-metal (ZG-209, Magnetic Shield Corp.). The homogeneity of our  $B_0$  and  $B_1$  fields were  $\pm 1\%$  over the NMR tube sample as measured using a magnetometer (Fluxgate-Magnetometer Fluxmaster, Stefan-Mayer Instruments, Germany) and are reported in Figure S2.

The  $B_1$  fields were generated in a custom-written Python software controlling the analog output of a digital-to-analog converter device (DAC, NI USB-6251, National Instruments, USA). The pulses were transmitted through a 12-Watt audio amplifier (KEMO MO32S) before reaching the  $B_1$  coil.

For the SABRE experiments, 5-mm medium-wall NMR tubes (Wilmad Labglass) were used to hold the samples. The tubes were connected to a gas injection setup based on previously published designs.<sup>[4,5]</sup> A water bath was situated within this setup to regulate the temperature of the samples, which were held in place during the experiment.

For the MRI experiments, the imaging device was a 7T preclinical MRI system (Biospec 70/20, PV6.0.1, Bruker, Germany), and the coil used was a proton-carbon quadrature-quadrature coil (V-XLS-HL-070-01349 V01, Rapid, Germany). The MRI sequences and protocols are reported below.

## SUPPORTING INFORMATION

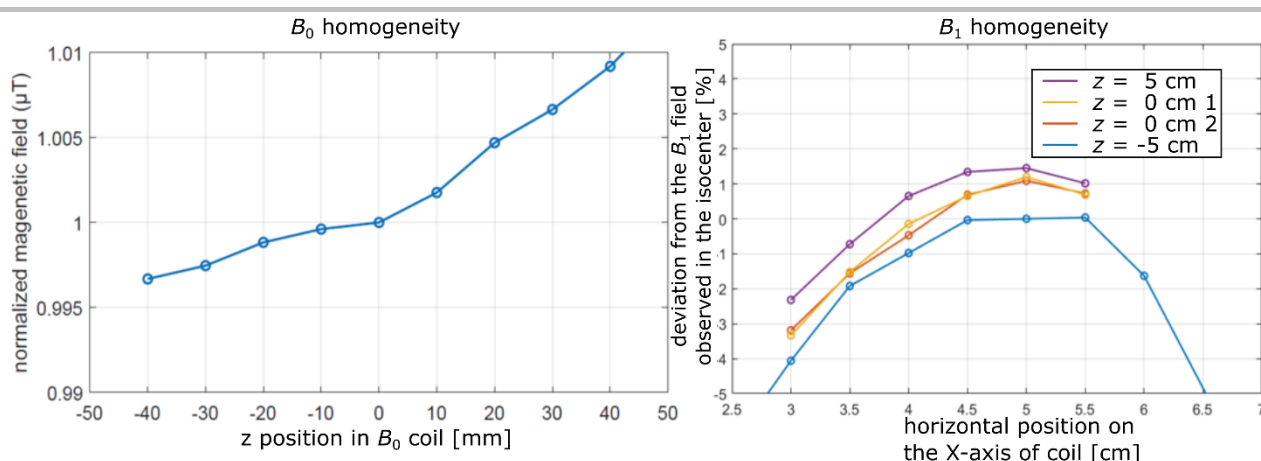


**Figure S2:** Relative offset of  $B_0$  along z-direction (left) and of  $B_1$  along x-direction measured at three distances along the z-direction (-5cm, 0cm, and +5cm from the center; right). 0cm was measured twice. X=5cm was the center of the  $B_1$  coil. Note that the samples were held in 5-mm NMR tubes that were aligned with the z-direction and had a fill height of approximately 6-8 cm during parahydrogen bubbling.

### Hyperpolarization Experiments

The NMR tubes were filled with 600  $\mu\text{L}$  of the SABRE solution. Initially, parahydrogen gas was introduced into the sample at 8 bar pressure for 2 minutes to activate the catalyst (Figure S3). Then, for the SABRE experiments, the samples were positioned in the experimental setup's water bath (approximately 5-10  $^{\circ}\text{C}$ , Figure S4).

After  $\approx 15$  s in the water bath, parahydrogen gas was passed through the solution, enabling polarization buildup with a time constant of approximately 1 min (Figure S5). Samples were hyperpolarized for 5 min by playing out the SLIC pulse while simultaneously guiding  $\text{pH}_2$  with 90% enrichment through the sample at  $\approx 8$  bar (Figure S1). While bubbling parahydrogen, the  $B_0$  and  $B_1$  fields were set to 50  $\mu\text{T}$  and 2  $\mu\text{T}$ , respectively. The sinusoidal oscillating  $B_1$  field with an amplitude of 2  $\mu\text{T}$  was applied to the sample at the Larmor frequency of the  $^{13}\text{C}$  spins ( $\omega = 535.25$  Hz). This process generated polarization that rotated with the magnetic field in the transverse plane.<sup>[6–12]</sup> Subsequently, a half passage adiabatic 90-degree pulse with an initial amplitude of 4  $\mu\text{T}$  was employed to align the magnetization parallel to the z-axis. During the pulse, the amplitude was gradually decreased from 4  $\mu\text{T}$  to 0 within 2 seconds, while the frequency of the  $B_1$  field was concurrently increased by 50 Hz.

To detect the hyperpolarized  $^{13}\text{C}$  signal using NMR, hyperpolarized samples were manually transferred to an 1T benchtop NMR spectrometer (SpinSolve Carbon 43, Magritek). The  $B_0$  field within the setup was maintained at 50  $\mu\text{T}$  during the transfer process and no further measures were taken to avoid zero-crossings when moving the sample out from the shield (i.e. no additional guiding field was applied to the mu-metal entrance).

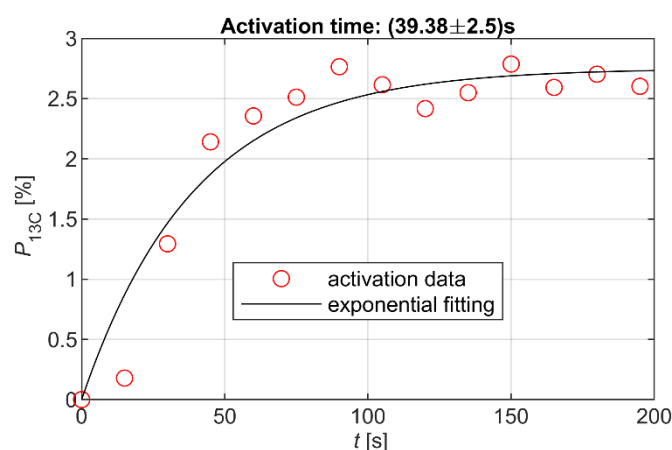


**Figure S3:**  $[1-^{13}\text{C}]$ -pyruvate- $\text{d}_3$  polarization measured at different times during the activation of the SABRE catalyst. Polarization levels are lower here, because the SABRE-SHEATH method, which yields lower  $^{13}\text{C}$ -polarizations for deuterated pyruvate,<sup>[12]</sup> was used for this specific sample.

## SUPPORTING INFORMATION

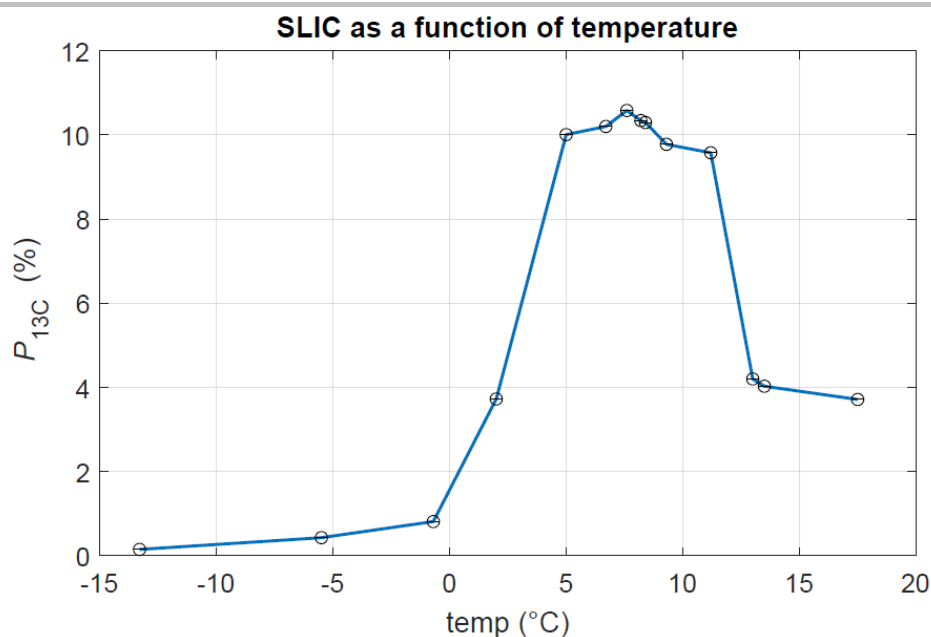


**Figure S4:** SLIC-SABRE hyperpolarization as function of temperature of the water bath.

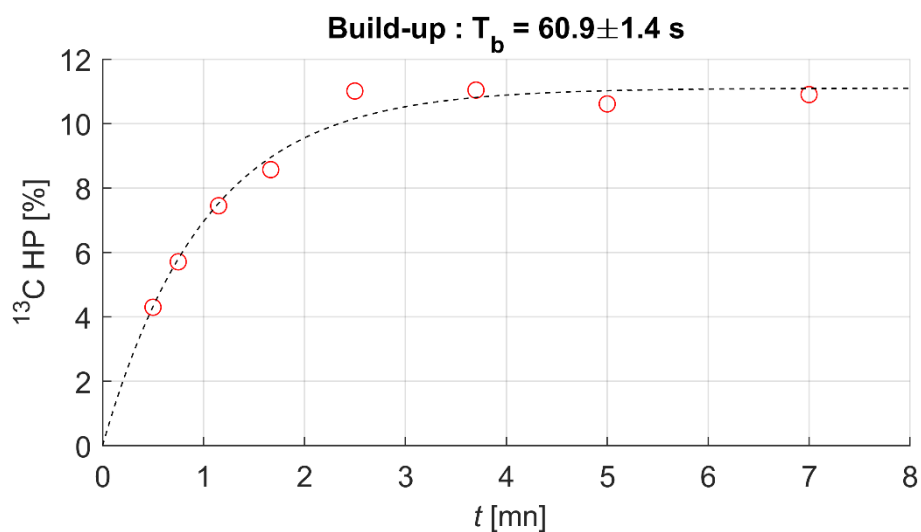


**Figure S5:** [ $1\text{-}^{13}C$ ]-pyruvate- $d_3$  polarization measured after different times of polarization build up. The build-up time constant was quantified to  $60.9 \pm 1.4$  s.

### Purification

After the SABRE hyperpolarization, we added 600  $\mu\text{L}$  phosphate-buffered  $D_2O$  (see SI) to the HP sample then placed it in a hot water bath and 450 mT magnetic field while applying vacuum (diaphragm pump, 2.4  $\text{m}^3/\text{h}$ , MZ2C, Vacuumbrand GmbH, Germany) from the top of the NMR tube. Subsequently, the solution was extracted through a 1.2  $\mu\text{m}$  syringe filter (Puradisc 13, Whatman, UK) using a 1 mL syringe combined with a catheter. The stepwise purification procedure is displayed in the main text Fig. 1d. Additionally, a schematic of the purification setup is presented in Figure S6.

## SUPPORTING INFORMATION

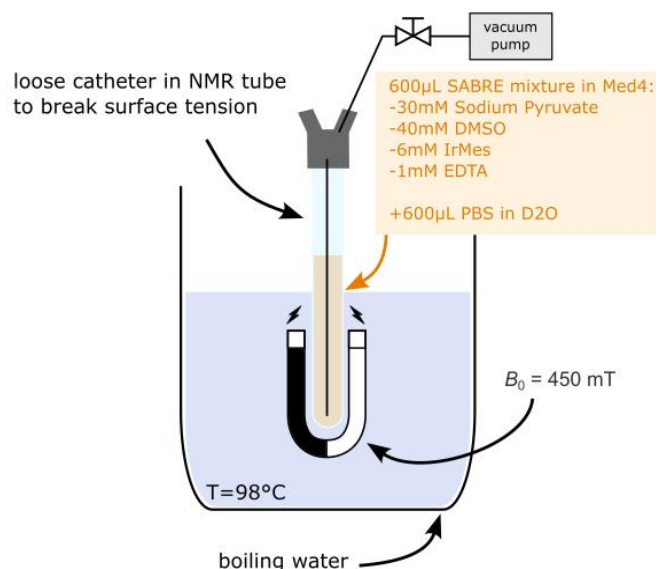


**Figure S6:** Schematic showing the purification setup.

### Concentration Determination

For non-purified samples, pyruvate concentrations were set by measuring the respective weights of the pyruvate before dissolving it in the according quantity of methanol- $d_4$ . These values (always 50 mM for non-purified samples) are reported in the main text. To determine the concentrations of pyruvate and methanol in purified samples, as well as their variations with evacuation time, we utilized the same setup and protocol for the purification of the SABRE solution (50 mM pyruvate, 40 mM DMSO, 1 mM EDTA, 6 mM SABRE catalyst in 600 μL of methanol), using protonated chemicals for  $^1\text{H}$  NMR analysis. The methanol- $\text{CH}_3$  signal in a spectrum acquired before evacuation served as an internal reference in the NMR spectra, and was calibrated to 12.35 M (after the addition of 600 μL of water to the 600 μL of methanol-based SABRE solution). The resulting NMR spectra are presented in Figure S7 and Figure S11, while the corresponding quantified data can be found in the main text Figure 2d and Figure S12.

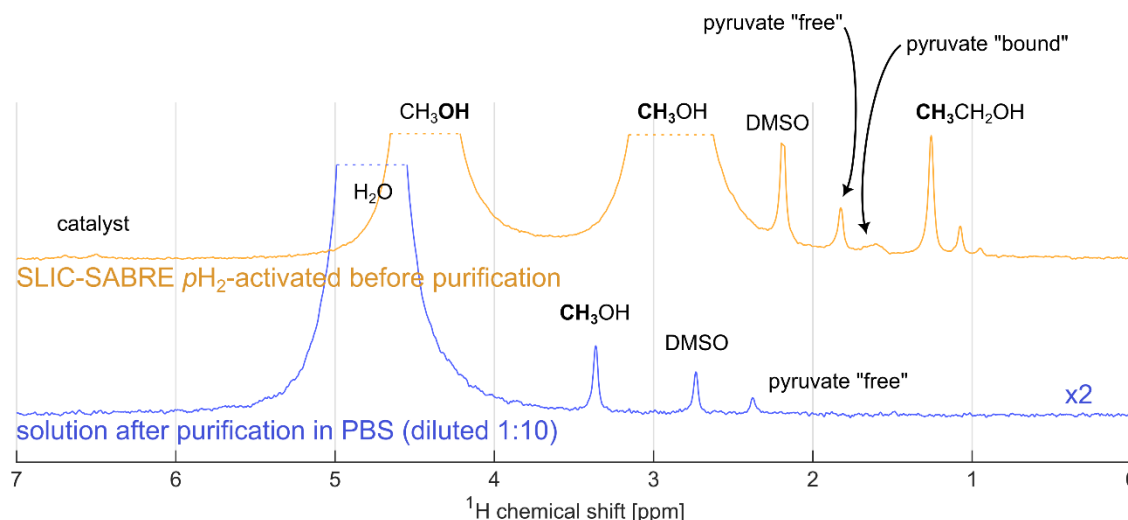


**Figure S7:** Example  $^1\text{H}$  NMR spectra of SABRE samples are shown before purification (top) and after purification using a  $\approx 5$  mbar vacuum and a  $98^\circ\text{C}$  water bath. These spectra were used to determine the final concentrations of methanol and pyruvate in purified solutions.

## SUPPORTING INFORMATION

## Polarization Calculation

The  $^{13}\text{C}$  polarization of hyperpolarized samples was quantified by calibration against a reference  $^{13}\text{C}$  signal of an external standard (neat  $[1\text{-}^{13}\text{C}]\text{acetic acid}$ , CAS: 1563-79-7, 99 atom %  $^{13}\text{C}$ , Sigma Aldrich) using the following formula:

$$P_{\text{hyp}} = \frac{S_{\text{hyp}}}{S_{\text{ref}}} \cdot \frac{[C_{\text{ref}}]}{[C_{\text{hyp}}]} \cdot \frac{N_{\text{ref}}}{N_{\text{hyp}}} \cdot \frac{f_{\text{ref}}}{f_{\text{hyp}}} \cdot P_{\text{ref}}$$

In this equation, "hyp" and "ref" denote the hyperpolarized sample and reference sample, respectively.  $S$  represents the integrated signal,  $[C]$  refers to the concentration, and  $f$  corresponds to the  $^{13}\text{C}$  fraction.  $N$  is the total number of acquired summations and was  $N = 1$  in all cases.  $P_{\text{ref}}$  is the Boltzmann thermal equilibrium polarization at room temperature (298 K) at the 1T magnetic field of the benchtop NMR system.

## In Vivo Experiments

The experimental procedures followed internationally accepted recommendations and guidelines for the handling of laboratory animals. Ethical approval for the animal experiments reported here was obtained from the relevant authority (Regierungspräsidium Freiburg, Talstr. 4-8, 79095 Freiburg; AZ: 35-9185.81/G-19/162). C57BL/6N mice with no genetic modifications weighing approximately 24 g were used for the study. Anesthesia was induced using sevoflurane (2-4% in >99.5%  $\text{O}_2$ ,  $\sim 1.0 \text{ L} \cdot \text{min}^{-1}$ , during spontaneous breathing) and the animal's vital signs were continuously monitored (SA Instruments 1030, Stony Brook, NY 11790). To maintain a respiration rate of about  $70 \text{ min}^{-1}$ , the anesthesia depth was adjusted as needed. Respiration was monitored using a pressure-sensitive cushion. The animal's body temperature was monitored using a rectal thermometer and stabilized using a custom-made water circulation system driven by a water pump. All necessary measures were taken to minimize the animal's suffering, and it was humanely euthanized at the end of the experiment.

 $^1\text{H}$  MRI Sequence and Parameters for Anatomical Reference:

Axial images: Multi-slice turbo-RARE,  $90/180^\circ$ , RARE-factor: 12, FOV:  $27.5 \times 20 \text{ mm}^2$ , matrix:  $100 \times 80$ , slice thickness: 1 mm, in-plane resolution:  $0.25 \text{ mm}^2$ ,  $TR = 4.73 \text{ s}$ ,  $TE = 6.33 \text{ ms}$ , 4 averages, acquisition time: 115s.

Coronal images: Multi-slice turbo-RARE,  $90/180^\circ$ , RARE-factor: 8, FOV:  $55 \times 27.5 \text{ mm}^2$ , matrix:  $200 \times 100$ , slice thickness: 1 mm, in-plane resolution:  $0.275 \text{ mm}^2$ ,  $TR = 4.0 \text{ s}$ ,  $TE = 6.33 \text{ ms}$ , 4 averages, acquisition time: 128s.

 $^{13}\text{C}$  CSI Sequence and Parameters:

Chemical Shift Images (CSI) were acquired with a center-out phase encode pattern. The excitation RF pulses were Shinnar-Le Roux pulses with sharpness 5, flip angle  $12^\circ$  and excitation bandwidth 8000 Hz. Imaging parameters were  $TR = 54 \text{ ms}$ ,  $TE = 1.04 \text{ ms}$ , spectral bandwidth 2000 Hz with 100 spectral points, resulting in 20 Hz spectral resolution. Slice thickness was 3 mm, FOV =  $30 \times 21 \text{ mm}^2$  and matrix size =  $20 \times 14$ , resulting in an in-plane voxel size of  $1.5 \times 1.5 \text{ mm}^2$ . Total acquisition time was 15.12 s. The acquisition was started 15 s post start of injection.

 $^{13}\text{C}$  Selective bSSFP Sequence and Parameters:

A spectrally-selective 3D balanced steady-state free precession sequence was used to selectively image pyruvate and lactate in an alternating pattern.<sup>[13]</sup> The sequence works by selectively exciting and refocusing the magnetization of a metabolite with a narrow-bandwidth off-resonant RF pulse while the signal is encoded with one read and two phase encode gradients. After acquiring one 3D image, the RF excitation frequency is alternated, and the other metabolite is targeted with an off resonant RF pulse.

The sequence was set to play constant-phase RF pulses and an  $\alpha/2$  -TR preparation pulse was used, with repetition time = 6.56 ms. The excitation RF pulse was a Shinnar-Le Roux pulse of sharpness 1 with 2.565 ms duration, excitation bandwidth 819 Hz and nominal flip angles of  $15^\circ$  (pyruvate) and  $60^\circ$  (lactate). The pyruvate targeting RF pulse center frequency was set -383 Hz off resonant from the pyruvate resonance ( $\sim 2.5$  passbands) and the lactate targeting RF pulse center frequency was set +537 Hz ( $\sim 3.5$  passbands) from the lactate resonance. FOV was  $56 \times 23 \times 21 \text{ mm}^3$ , matrix size =  $56 \times 23 \times 21$ , voxel size =  $1 \times 1 \times 1 \text{ mm}^3$  for the phantom measurement and FOV =  $55 \times 27.5 \times 20 \text{ mm}^3$ , matrix size =  $21 \times 11 \times 8$ , voxel size =  $2.5 \times 2.5 \times 2.5 \text{ mm}^3$  for the in vivo measurement. The measurement was started  $\sim 15\text{s}$  before start of injection and 250 repetitions were acquired.



## SUPPORTING INFORMATION

**<sup>13</sup>C MRI data processing and visualization:**

The postprocessing of the <sup>13</sup>C images displayed in the main text is described in the following; non-interpolated and non-windowed images are presented in Figure S17 and Figure S18. First, metabolite maps were interpolated from their original voxel size to correspond to the one of the anatomical <sup>1</sup>H images. The Matlab function 'imresize' with bilinear interpolation was employed for this purpose. Subsequently, the metabolite maps were normalized so that the pixel with the lowest intensity and the one with the highest intensity are assigned values of 0 and 1, respectively. Gray level metabolite maps were then converted into color images using the 'ind2rgb' function in Matlab. Custom color maps were created for each metabolite, starting with black and ending with white, and incorporating a metabolite-specific color (shown in the corresponding main text figures). Finally, the anatomical image was superimposed with the metabolite map. To this end, the <sup>13</sup>C images were windowed by calculating a transparency factor based on the pixel intensity of the metabolite map. This factor was adjusted for each metabolite to achieve optimal visualization of both metabolism and anatomy. The transparency functions used for the metabolite maps presented in main text Figure 3 and Figure 4, which were obtained using a chemical shift imaging sequence and a frequency-selective bSSFP imaging method, respectively, are presented in Figure S8.

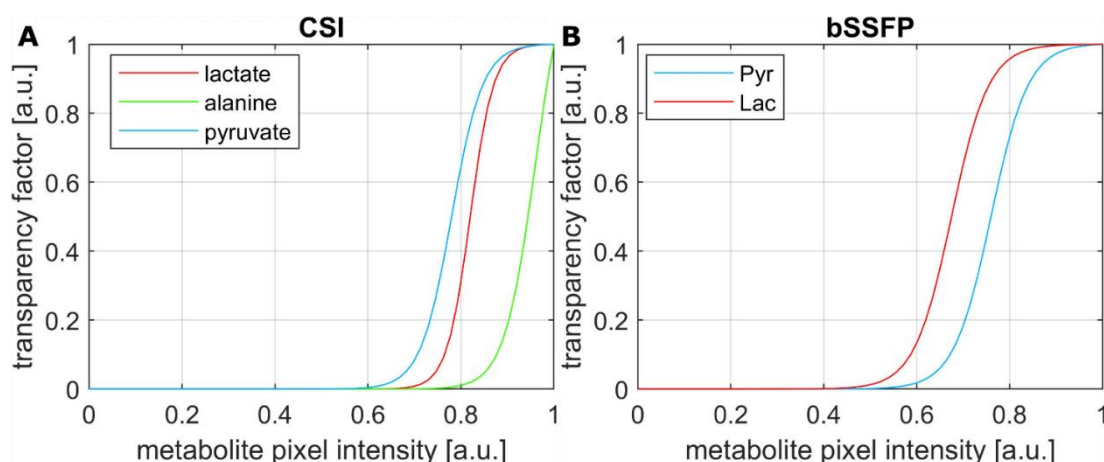


**Figure S8:** Signal transparency factor applied to <sup>13</sup>C metabolite maps presented in the main text Figure 3 and Figure 4 to display them co-registered with the anatomical <sup>1</sup>H MRI images. The blue curve, the red curve show the transparency correspondence factor of pyruvate and lactate, respectively.

## Analysis of the Purified Hyperpolarized Solutions

Photos of the NMR tube at different steps of the purification and of extracted solutions are presented in Figure S9. Purified SABRE samples were analyzed for their biocompatibility. Osmolarity and pH were adjusted using the PBS described in sample preparation above. Additionally, the **pH** was investigated in 10 samples using pH strips and additionally with a pH meter (Figure S10). **Methanol and pyruvate concentrations** reported in main text Fig. 2d were determined with <sup>1</sup>H NMR spectroscopy (Figure S7 and Figure S11). In addition to the data reported in the main text Fig. 2d, we tested the evaporation using the same vacuum pump in an 80°C water bath as shown in Figure S12. Note that in these experiments reported in Figure S12, the sample contained no SABRE catalyst, EDTA, and DMSO, but only 50mM pyruvate in methanol-OH. We found that evaporation was slower at 80°C compared to 100°C and similar methanol concentrations were found only after approximately twice the time. **Sterility** was investigated by spreading 400μl of the purified samples on agar plates free of antibiotics and incubating them for 48 hours as described in the caption of Figure S13. Residual iridium in purified samples was investigated with inductively coupled plasma optical emission spectroscopy (ICP-OES) and in samples where methanol was evaporated for 15s at 98°C or for 30s at 80°C we found 3.9 mg/L iridium and 2.96 mg/L iridium, respectively. Considering the mass of iridium of 192.217 u, these values correspond to final concentrations of 20.3 μM and 15.4 μM, respectively. **Cytotoxicity** of purified solutions and assays with different concentrations of methanol, pyruvate, PBS, D<sub>2</sub>O, and iridium-based SABRE catalyst was investigated as described in the next paragraph and as reported in Figure S14.

## Cell culture and MTT for cytotoxicity

An MTT assay was used to investigate the cytotoxicity of the purified SABRE solution. The MTT assay is a commonly used colorimetric assay to investigate cell metabolic activity after treatment (doi:10.1101/pdb.prot095505). It is based on the conversion of MTT (3-(4,5-dimethylthiazol-2-yl)-2,5-diphenyltetrazolium bromide) to formazan via the enzyme oxidoreductase. The purple formazan can be solved in DMSO and the colored solution can then be quantified by a spectrophotometer. For the presented project, PyB6-313 murine breast cancer cells were used and following conditions, cell culture and MTT procedures were performed.

## SUPPORTING INFORMATION

**Cultivation conditions:** - Cells were cultured in 10cm cell culture dishes at 37°C and 5% CO<sub>2</sub> in DMEM Medium (gibco – 41966029) supplemented with 10% FCS (PAN Biotech - P30-3306), 1% L-Glutamine (Sigma-Aldrich – G7513) and 1% Penicillin/Streptomycin (gibco – 11548876).

**Splitting of cells:** When a confluency of >80% was reached, the medium was removed and the cells were washed once with DPBS (gibco – 14190094), 1ml of 0.05% Trypsin-EDTA (gibco – 25300054) was added and cells were incubated for 10min at 37°C, 4ml of cell culture medium (described above) was added and cells were transferred to a new dish (1:10).

**MTT:** Cells were detached as described in “splitting of cells”, seeded into a 96-well plate at  $3 \times 10^3$  cells/well and incubated at 37°C and 5% CO<sub>2</sub> overnight. The medium was removed and treatment was started by addition of 120µl of prepared treatment media as described in Figure S14. After 24h/48h of incubation, medium was removed, 120µl MTT medium ((1:10) MTT (5 mg/ml: abcam – AB14345) : indicator free cell culture medium (PAN Biotech – P04- 03591)) was added and the plates were incubated for 2:20h at 37°C and 5% CO<sub>2</sub>. After incubation the MTT medium was removed and 120µl DMSO were added, followed by 20min incubation at RT in motion. Finally, absorption at 570nm (reference absorption: 630nm) was measured using an EnSpire multimode plate reader to quantify the formazan formation as a measure of cell viability.

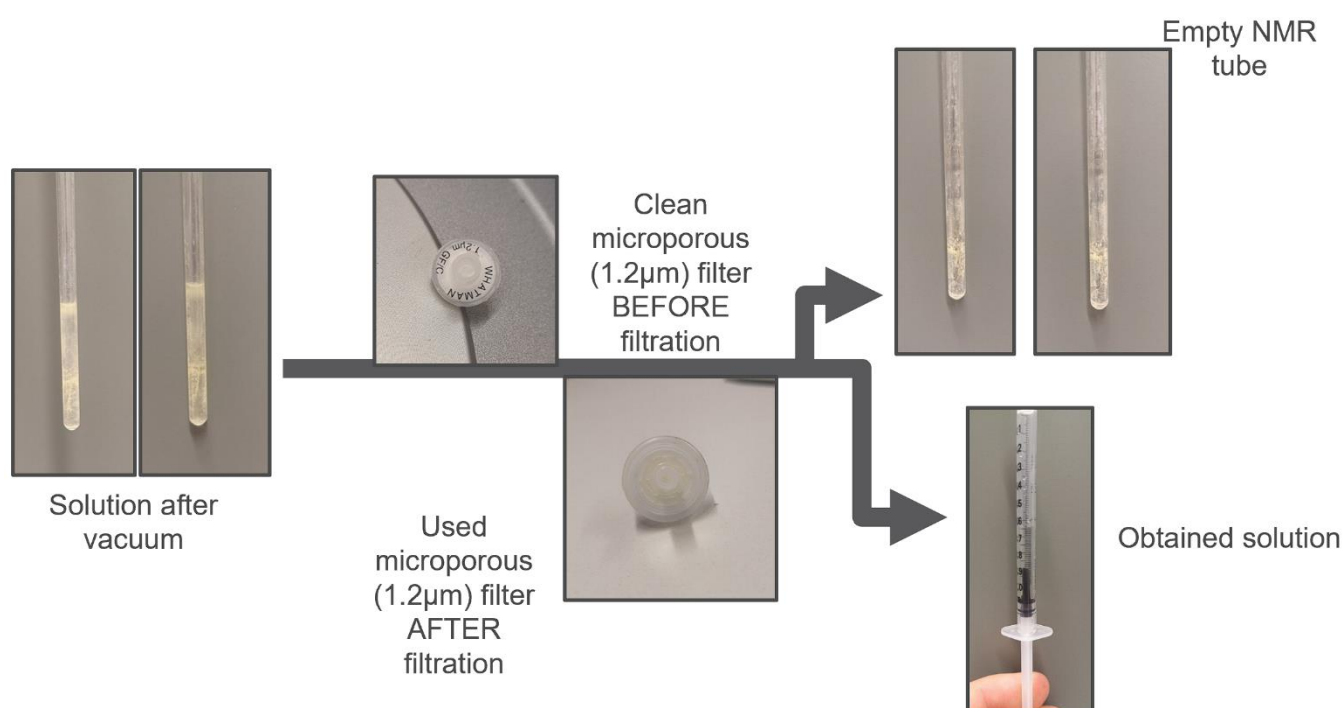


**Figure S9:** Photos collected after solvent evaporation before and after filtering the SABRE solutions.

## SUPPORTING INFORMATION



**Figure S10:** pH of the purified samples. The pH determined using pH stripes was reproducibly at  $7.5 \pm 0.1$  as evaluated in 10 experiments (error estimated). The individual sample size was too small for using an electronic high precision pH meter. However, pH of 7.5 was confirmed from a batch collected from 10 individual purified samples.

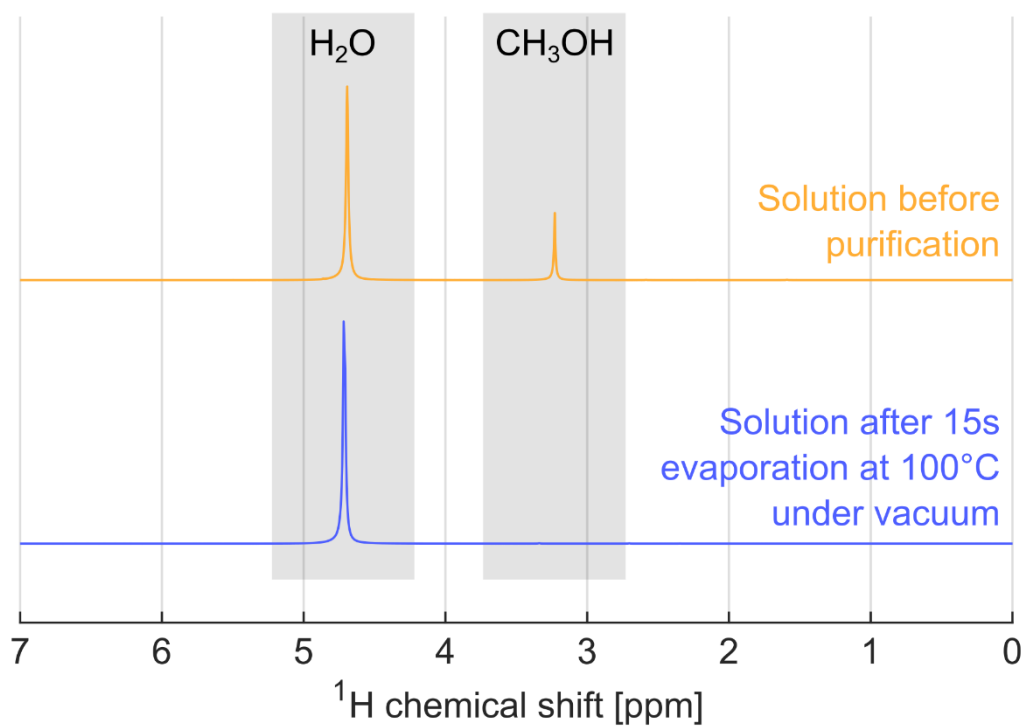


**Figure S11:** Example  $^1\text{H}$  NMR spectra of methanol and pyruvate before and after 15s solvent evaporation.

## SUPPORTING INFORMATION

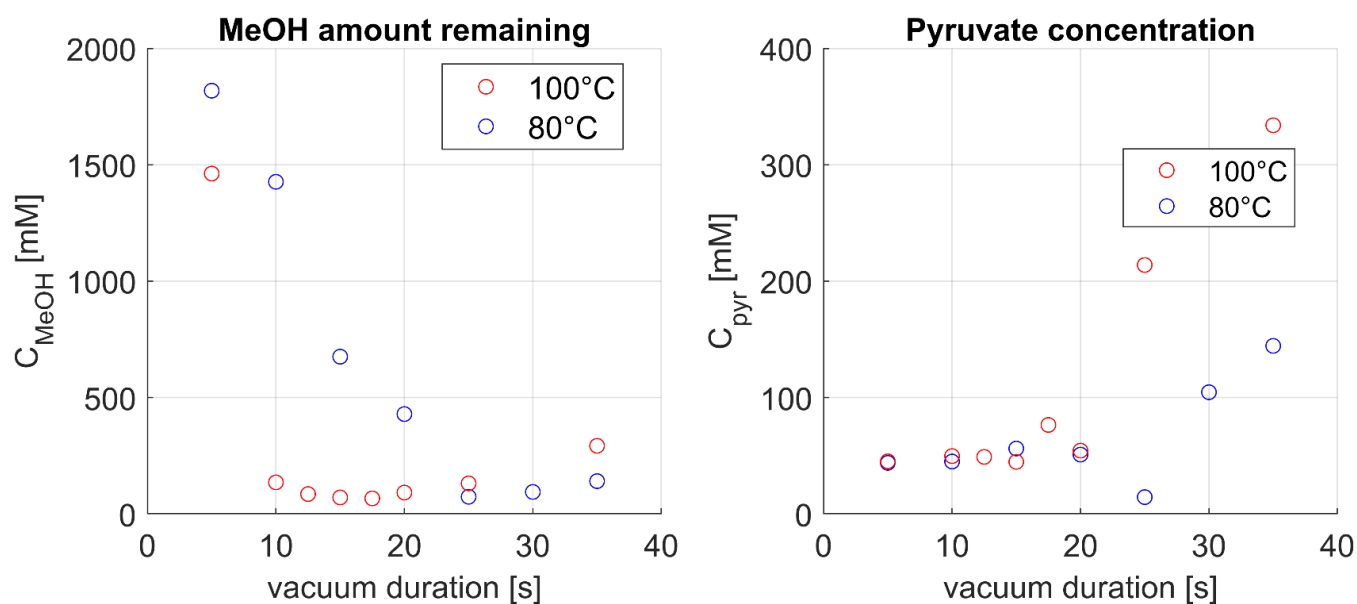


**Figure S12:** Methanol and pyruvate concentrations measured after different times of vacuum and at either 80°C or 98°C water bath temperature. Note that data presented here was acquired using  $^1\text{H}$  NMR and samples of 50mM sodium pyruvate- $\text{h}_3$  in 600 $\mu\text{L}$  methanol-OH mixed with 600 $\mu\text{L}$   $\text{H}_2\text{O}$  (without SABRE catalyst, EDTA, and DMSO).

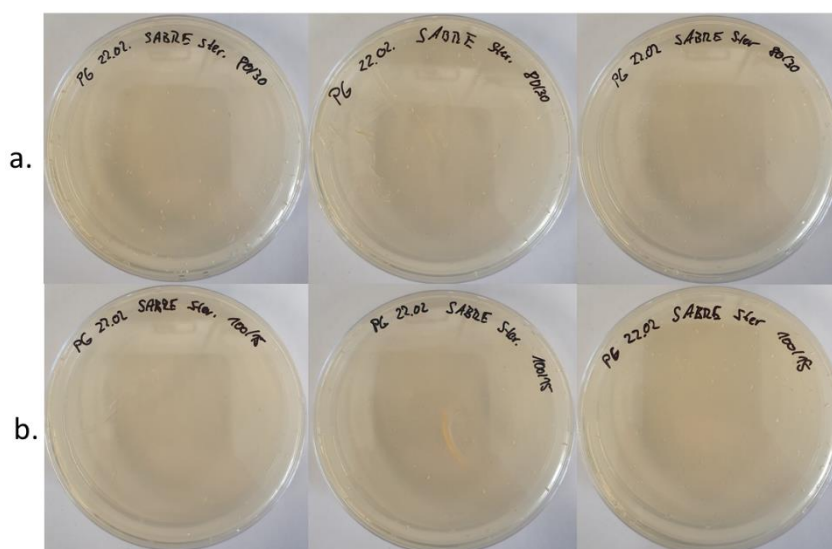


**Figure S13:** Sterility analysis of purified SABRE solution. The sterility was investigated by spreading 400 $\mu\text{L}$  of the respective samples (line a.: 30s purification at 80°C, line b.: 15s purification at 100°C) on agar plates, free of antibiotics. The plates were incubated at 37°C for 48h and visually inspected for any kind of colony formation. No growth of bacteria or fungi was observed.

## SUPPORTING INFORMATION

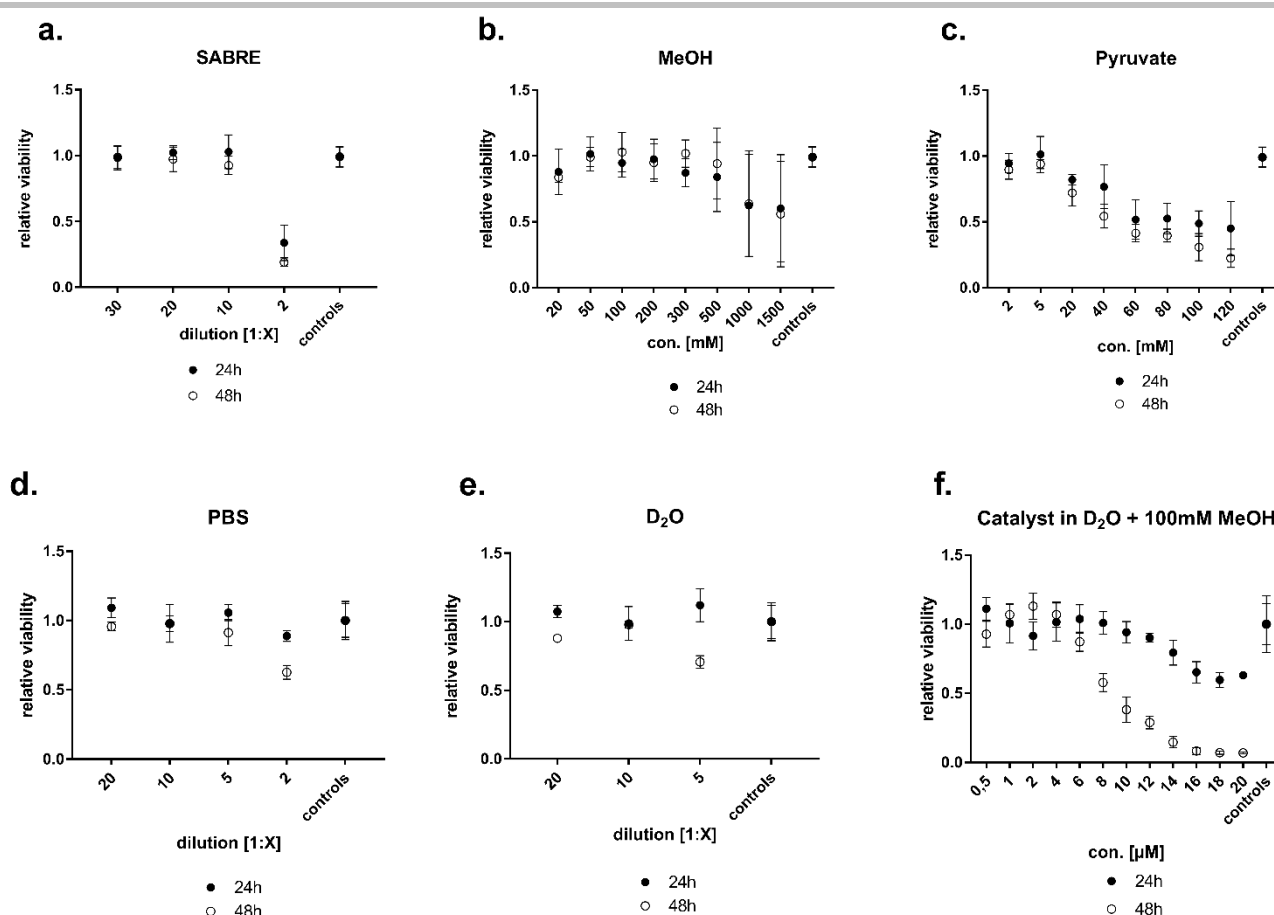


**Figure S14:** Cytotoxicity test of purified SABRE samples (a) in comparison with methanol (b), pyruvate (c), PBS (d), D<sub>2</sub>O (e) and catalyst solution (f) using MTT assay. The SABRE solutions (15s evaporation at 100°C followed by microporous filtration) were pooled from several individual purifications and diluted with cell culture medium at the indicated dilution factor. The Methanol (MeOH), Pyruvate, PBS, D<sub>2</sub>O and catalyst solutions were made via dilution of stock solutions of the highest concentration with cell culture medium and subsequent dilution. The exact MTT procedure is described above (same section in the SI). Three biological replicates were done for experiments a-c (started at 3 different days) with technical triplicates (every condition three replicates per run), the two lowest concentrations of pyruvate and methanol were added at the second biological replicate. Experiments d-e consisted of one biological replicate with three technical triplicates. Values of 24h and 48h time points are normalized to their corresponding control, which was untreated. Plot a. shows, that the SABRE solution, at physiological dilutions (1:30, 1:20, 1:10), has only minor effects on cell viability. Only the 1:2 dilution reduces cell viability significantly. In plot b. it is demonstrated that only higher methanol concentrations (>500mM) reduce cell viability, regardless of the treatment time. Pyruvate however (shown in plot c.) decreases cell viability upon a concentration of 20mM. Plots d. and e. show that the nutrient withdrawal, caused by culture media dilution, has minor effects on the viability, although a 1:2 dilution (1:5 for neat D<sub>2</sub>O, plot e) reduced viability after 48h. Those results, combined with the data shown in plot f. suggest, that the toxicity of the SABRE solution at 1:2 dilution likely arises mostly from the remaining iridium-based catalyst in the solution (≈10μM at 1:2 dilution), a relatively high pyruvate concentration (≈15mM, see (c)), and dilution of the cell medium (compare with (d))

## MRI experiments

Before using the purified HP pyruvate solutions in animals, we tested the injection and <sup>13</sup>C imaging in a test object similar to our previous study (Figure S15).<sup>[14]</sup> This phantom is described in the following: A thin silicone tube (2 mm OD x 1 mm ID) was attached to the end of a 1 mL syringe. It is worth noting that the diameter of an adult mouse's aorta is approximately 1.2 mm.<sup>[15]</sup> The tube was coiled around the syringe, and both were mounted inside a 15 mL polypropylene (PP) Falcon tube. The syringe plunger and the PTFE tube end were threaded through the Falcon wall, which was sealed with epoxy adhesive. The Falcon tube was filled with deionized water for magnetic field shimming and <sup>1</sup>H-MRI for image co-registration. The PTFE hose end was connected to a catheter that was connected with a 30G cannula for the injection. During injections into this test object, the hose would fill first, followed by the syringe inside the test object. The injection would then push the plunger out, simulating a finite backpressure during *in vivo* administration. After the imaging experiment, the test object was emptied by pushing the plunger back in. To remove the catalyst-substrate solutions, the test object was filled with deionized water and emptied three times.

For reference, a <sup>13</sup>C enriched sample solution of 4M [1-<sup>13</sup>C]-lactate in H<sub>2</sub>O doped with gadolinium (2 mM DOTAREM) was used. In the MRI experiments, this sample was positioned next to the imaging phantom or mice.

The Fourier-transformed non-interpolated and non-windowed data of the <sup>13</sup>C CSI reported in main text Fig. 3 is presented in Figure S16 and Figure S17. Likewise, the non-interpolated and non-windowed data acquired with the frequency-selective bSSFP sequence

## SUPPORTING INFORMATION

presented in main text Fig. 4 is shown in Figure S18. The animal monitoring data was recorded during the injection and is shown in Figure S19.

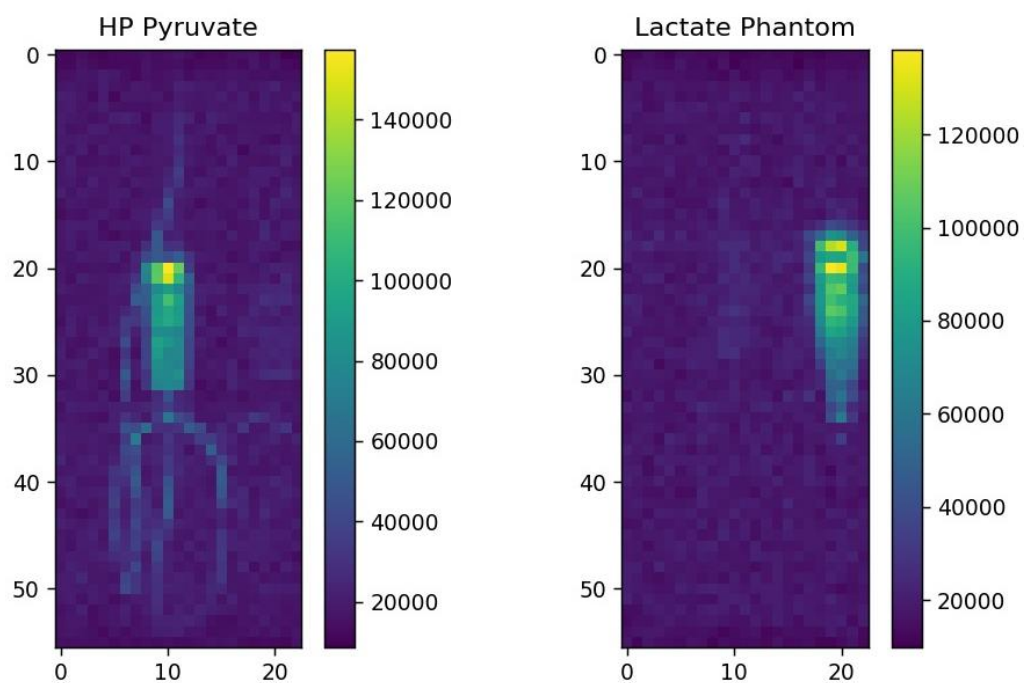


**Figure S15:** Example 7T  $^{13}\text{C}$  MRI of HP  $[1\text{-}^{13}\text{C}]$ -pyruvate- $\text{d}_3$  in an imaging test object and a  $[1\text{-}^{13}\text{C}]$ -lactate reference solution.



## SUPPORTING INFORMATION

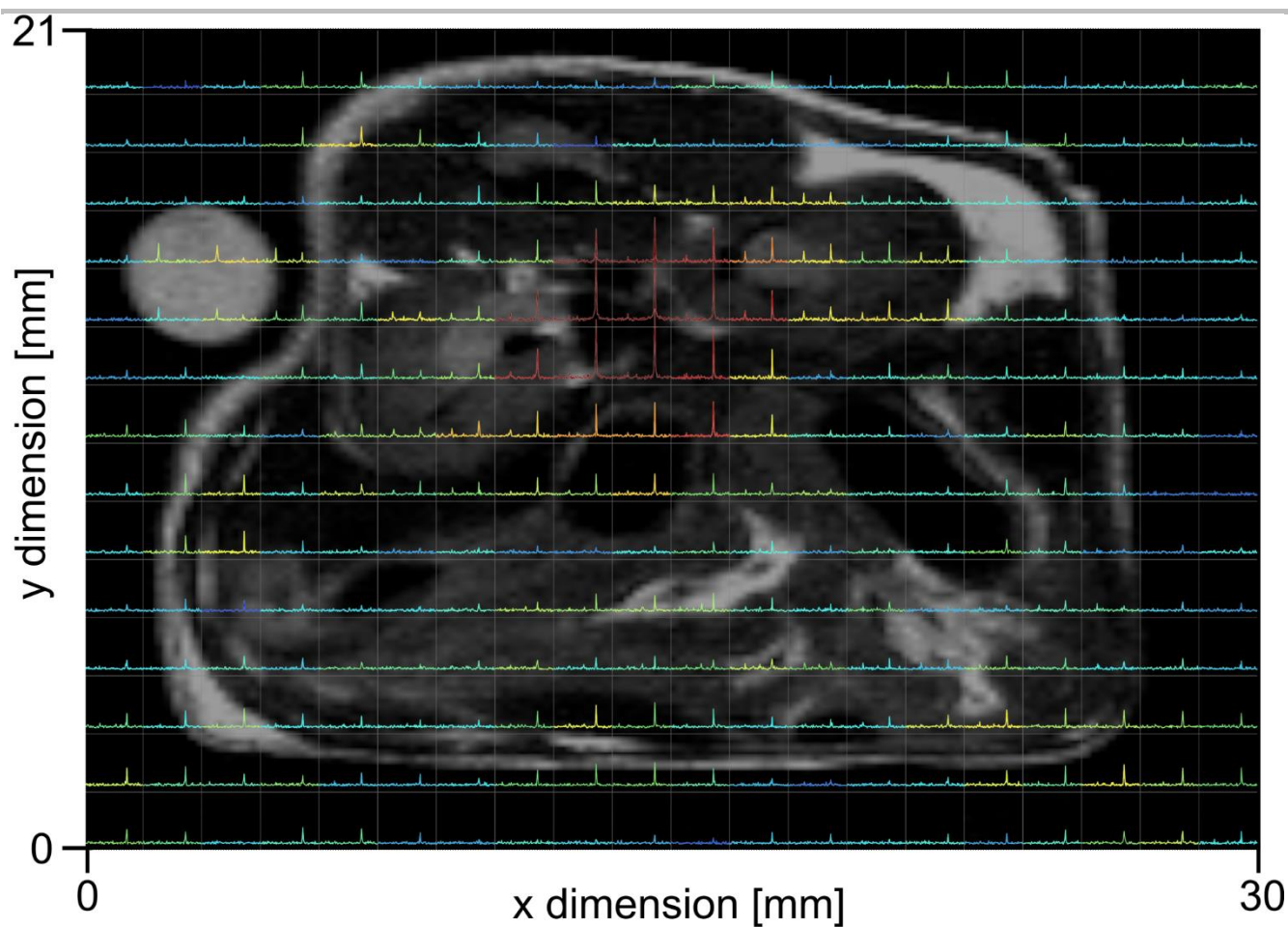


**Figure S16:** Localized hyperpolarized  $^{13}\text{C}$  spectra obtained with the CSI measurement reported in main text Fig. 3.

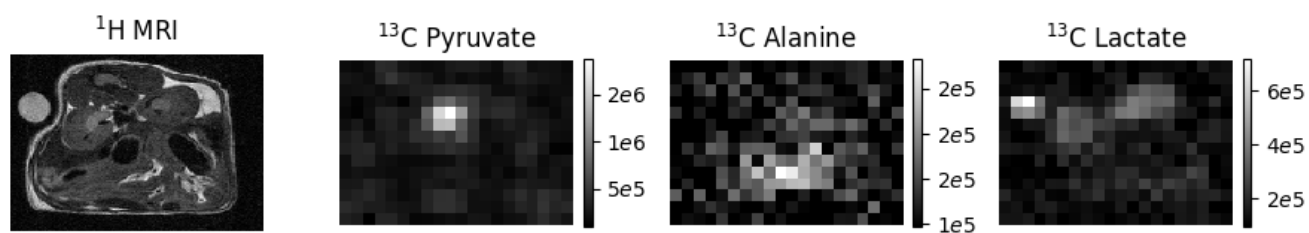


**Figure S17:**  $^{13}\text{C}$  CSI images of the single metabolites as reported in main text Fig. 3 but without interpolation and windowing.

## SUPPORTING INFORMATION

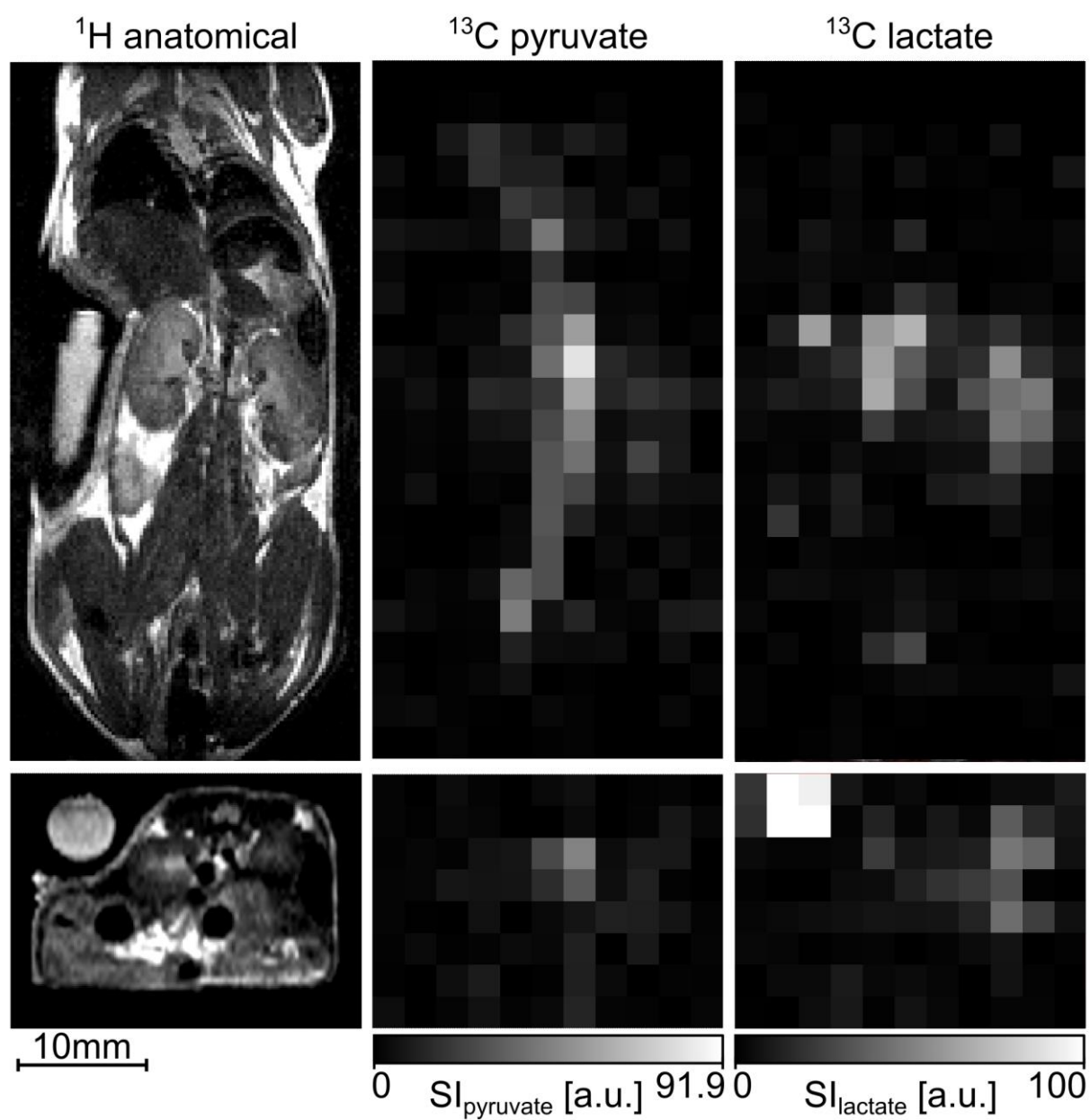


**Figure S18:**  $^{13}\text{C}$  bSSFP images of the single metabolites as reported in main text Fig. 4 but without interpolation and windowing.



## SUPPORTING INFORMATION

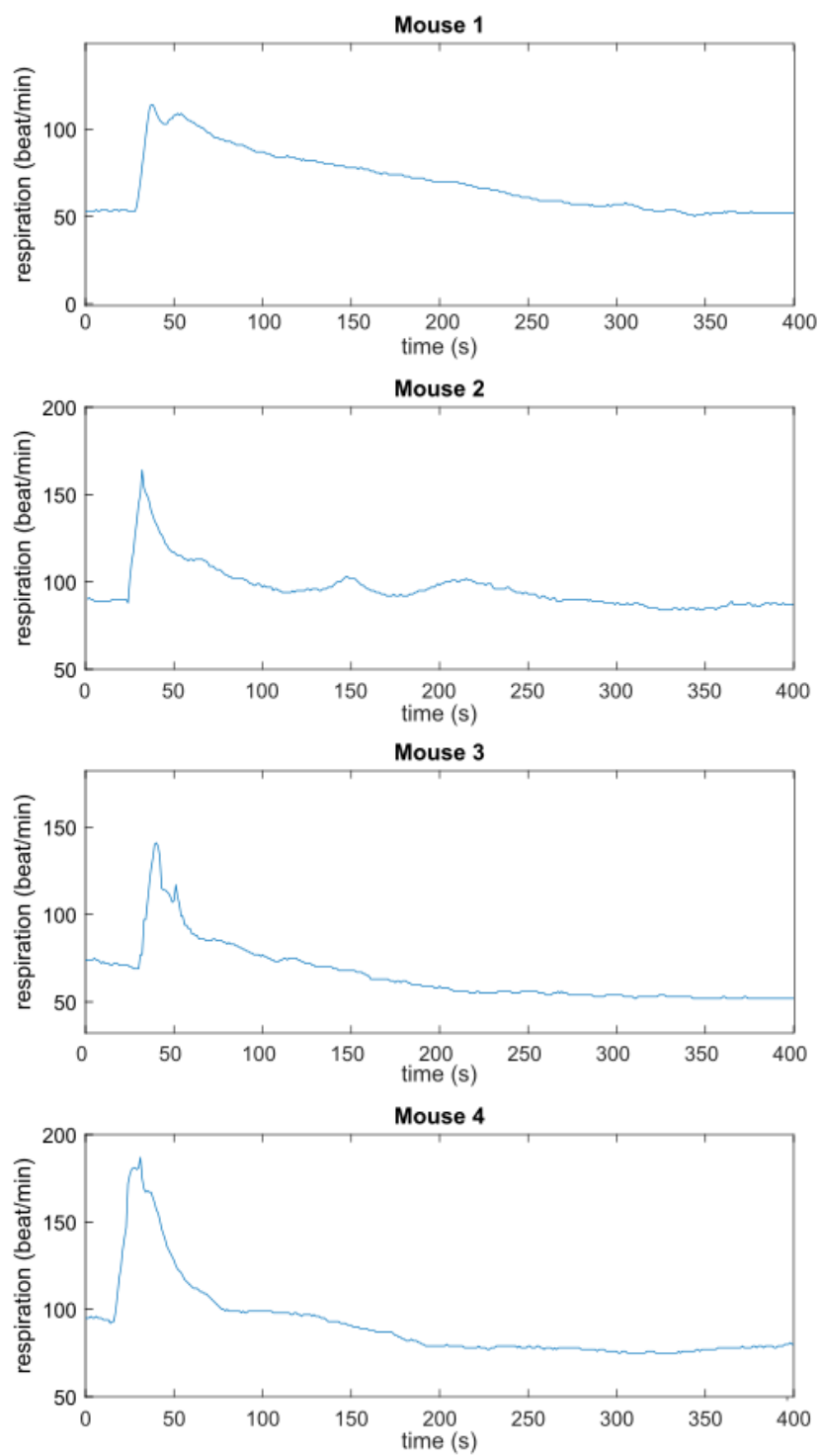


**Figure S19:** Animal monitoring data showing the time of injection of the HP pyruvate and the temporary increase of the breathing rate.

## SUPPORTING INFORMATION

Relaxation Data Used to Determine  $T_1$  and  $T_{1\rho}$  at Different Magnetic Fields

Here we report the decay curves used to determine  $^{13}\text{C}$   $T_1$  and  $T_{1\rho}$  values of  $[1-^{13}\text{C}]$ -pyruvate- $\text{d}_3$  reported in the main text Fig. 2c. Relaxation was monitored in methanol- $\text{d}_4$  based SABRE solution (see section 1 for concentrations), and in phosphate-buffered  $\text{D}_2\text{O}$  and phosphate-buffered  $\text{H}_2\text{O}$  at 7T (Figure S20), 1T (Figure S21), 450mT (Figure S22), and at 50 $\mu\text{T}$  (Figure S23). Note that relaxation data in PBS  $\text{H}_2\text{O}$  and  $\text{D}_2\text{O}$  at 50 $\mu\text{T}$  and 450mT was acquired from non-hyperpolarized pyruvate using a field-cycling device coupled to a 400MHz NMR spectrometer (Bruker).

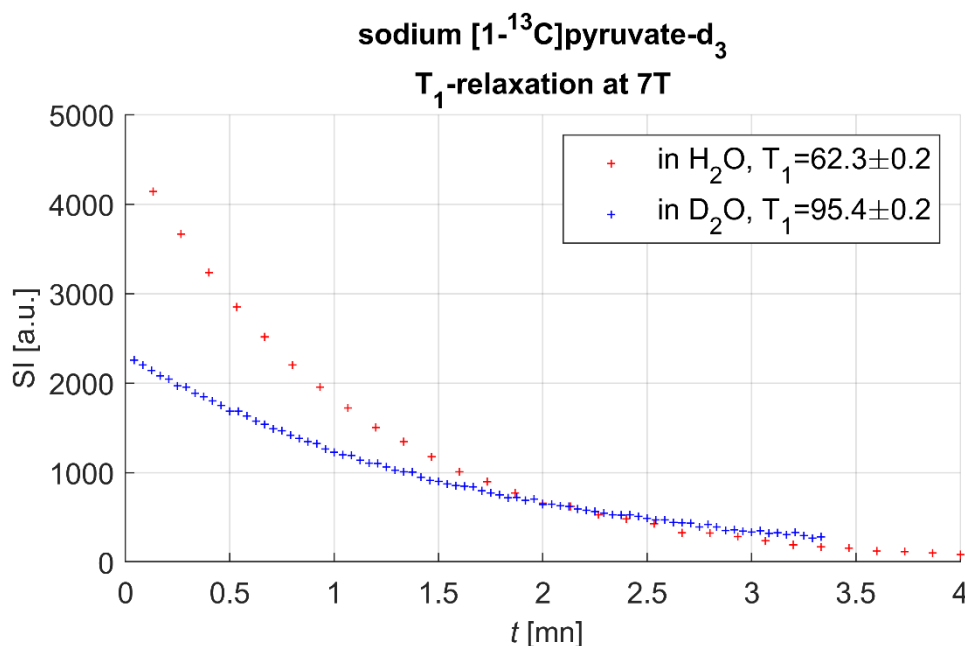


**Figure S20:** Longitudinal relaxation of hyperpolarized  $[1-^{13}\text{C}]$ pyruvate- $\text{d}_3$  at 7T in phosphate-buffered  $\text{D}_2\text{O}$  or  $\text{H}_2\text{O}$  at pH 7.5. The  $T_1$  data was recorded from SLIC-SABRE hyperpolarized samples; the aqueous samples were purified using the protocol described in the main text. The samples were held in an NMR tube and placed in the 7T preclinical MRI system used for imaging experiments. NMR spectra were recorded using a series of pulse-detect experiments with a 10 degree flip angle. The effect of the flip angle was corrected for the data reported here.

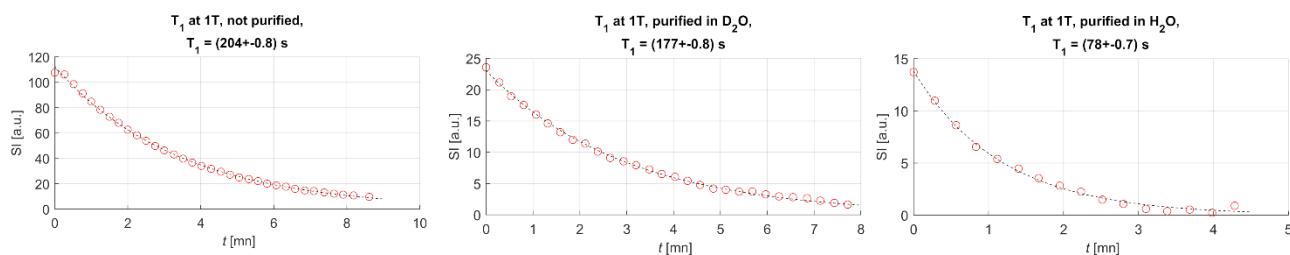


**Figure S21:** Longitudinal relaxation of hyperpolarized  $[1-^{13}\text{C}]$ pyruvate- $\text{d}_3$  at 1T in methanol- $\text{d}_4$ , and phosphate-buffered  $\text{D}_2\text{O}$  or  $\text{H}_2\text{O}$  at pH 7.5. The  $T_1$  data was recorded from SLIC-SABRE hyperpolarized samples; the aqueous samples were purified using the protocol described in the main text. The samples were held in an NMR tube and placed in the 1T benchtop NMR spectrometer. NMR spectra were recorded using a series of pulse-detect experiments with a 10 degree flip angle. The effect of the flip angle was corrected for the data reported here.

## SUPPORTING INFORMATION

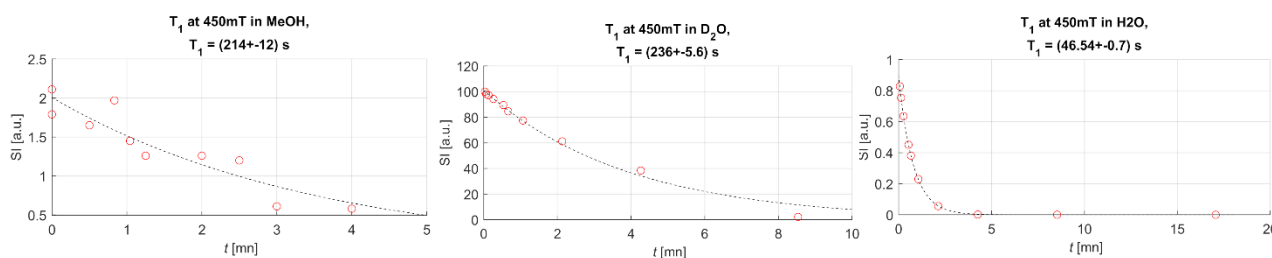


**Figure S22:** Longitudinal relaxation of hyperpolarized  $[1\text{-}^{13}\text{C}]\text{pyruvate-d}_3$  at 450mT in methanol- $\text{d}_4$ , and phosphate-buffered  $\text{D}_2\text{O}$  or  $\text{H}_2\text{O}$  at pH 7.5. In case of methanol- $\text{d}_4$ , the  $T_1$  data was recorded from a SLIC-SABRE hyperpolarized sample. For each data point this sample was hyperpolarized, then moved in the field of the 450mT magnet for varying amount of time, then transferred to the 1T benchtop NMR spectrometer for detection. Data for the  $T_1$  relaxation in phosphate-buffered  $\text{D}_2\text{O}$  and  $\text{H}_2\text{O}$  was recorded from thermally polarized samples using a field cycling setup.

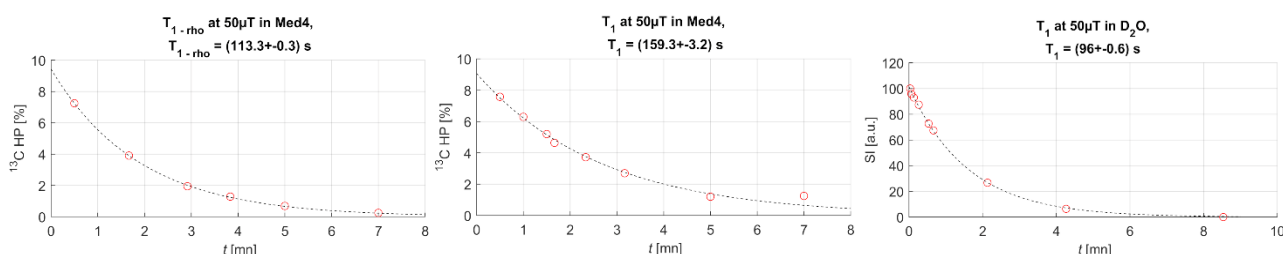


**Figure S23:** Longitudinal relaxation of hyperpolarized  $[1\text{-}^{13}\text{C}]\text{pyruvate-d}_3$  at 50 $\mu\text{T}$  in methanol- $\text{d}_4$  in absence and , and phosphate-buffered  $\text{D}_2\text{O}$  at pH 7.5, and  $T_{1\rho}$  relaxation in presence of the SLIC pulse in methanol- $\text{d}_4$ . For each data point in the measurement of  $T_1$  in methanol, the sample was hyperpolarized using SLIC-SABRE and polarization was rotated along the 50 $\mu\text{T}$  field using an adiabatic pulse as described in the main text. Then, the sample was rested in the 50 $\mu\text{T}$  field for a variable time before transferring it to the 1T NMR benchtop spectrometer for detection. For the  $T_{1\rho}$  measurement, the SLIC pulse with spin-lock amplitude of  $B_1 = 2\text{ }\mu\text{T}$  was played out for a variable duration, but  $\text{pH}_2$  was only bubbled through the sample for the first 60s. Data for the  $T_1$  relaxation in phosphate-buffered  $\text{D}_2\text{O}$  was recorded from thermally polarized samples using a field cycling setup.

## Remaining Methanol and Iridium with Respect to a Potential Human Translation

We would like to clarify that our study does not aim to develop or produce contrast agents suitable for human use. However, considering the potential future application of our technique in patient studies, it is important to acknowledge the current safety limitations. The international council for harmonization (ICH), which comprises international regulators including the FDA and EMA, provides guidelines that include limits on residual organic solvents and elements for the use of pharmaceuticals in humans.

**Methanol:** The ICH considers a fraction of 3,000 ppm of methanol in the administered dose to be safe.<sup>[16]</sup> Taking into account the residual 250 mM methanol present in our purified solutions, we calculate a concentration of approximately 7,950 ppm (or 7,280 ppm when accounting for isotope labelling) via the formula:

$$\text{Concentration [ppm]} = \frac{m_{\text{methanol}}}{m_{\text{dose}}} = \frac{c_{\text{methanol}} \cdot M_{\text{methanol}}}{c_{\text{methanol}} \cdot M_{\text{methanol}} + c_{\text{water}} \cdot M_{\text{water}}}$$

The variables  $m$ ,  $c$ , and  $M$  correspond to the mass, concentration, and molar weight, respectively, with the indices referring to either methanol or water. Notably, this value is approximately three times higher than the level suggested by ICH as acceptable for human use.

**Iridium:** According to the ICH guidelines, the permitted daily exposure (PDE) for iridium is specified as 10  $\mu\text{g}$ .<sup>[17]</sup> After purification, the residual concentration of iridium-based catalyst in our HP solutions was measured to be 20  $\mu\text{M}$ . Considering that larger injection volumes are typically used for patient applications, such as 50 mL<sup>[18]</sup>, our current formulation would result in an approximate amount of 50 mL  $\times$  20  $\mu\text{M}$   $\times$  192 g/mol = 192  $\mu\text{g}$  of iridium. Therefore, to ensure safety in patients and to meet the PDE, the concentration of iridium would need to be reduced by approximately 20-fold.

## SUPPORTING INFORMATION

## References Used in Supporting Information

- [1] J.-B. Hoeverner, S. Bär, J. Leupold, K. Jenne, D. Leibfritz, J. Hennig, S. B. Duckett, D. von Elverfeldt, *NMR Biomed.* **2013**, *26*, 124–131.
- [2] R. Savka, H. Plenio, *Dalton Trans.* **2015**, *44*, 891–893.
- [3] A. B. Schmidt, D. L. Andrews, A. Rohrbach, C. Gohn-Kreuz, V. N. Shatokhin, V. G. Kiselev, J. Hennig, D. von Elverfeldt, J.-B. Hövener, *J. Magn. Reson.* **2016**, *268*, 58–67.
- [4] A. S. Kiryutin, G. Sauer, S. Hadjiali, A. V. Yurkovskaya, H. Breitzke, G. Buntkowsky, *J. Magn. Reson.* **2017**, *285*, 26–36.
- [5] A. B. Schmidt, H. de Maissin, I. Adelabu, S. Nantogma, J. Ettegui, P. TomHon, B. M. Goodson, T. Theis, E. Y. Chekmenev, *ACS Sens.* **2022**, *7*, 3430–3439.
- [6] S. J. DeVience, R. L. Walsworth, M. S. Rosen, *Phys. Rev. Lett.* **2013**, *111*, 173002.
- [7] T. Theis, M. Truong, A. M. Coffey, E. Y. Chekmenev, W. S. Warren, *J. Magn. Reson.* **2014**, *248*, 23–26.
- [8] A. N. Pravdivtsev, I. V. Skovpin, A. I. Svyatova, N. V. Chukanov, L. M. Kovtunova, V. I. Bukhtiyarov, E. Y. Chekmenev, K. V. Kovtunov, I. V. Koptug, J.-B. Hövener, *J. Phys. Chem. A* **2018**, *122*, 9107–9114.
- [9] S. Knecht, A. S. Kiryutin, A. V. Yurkovskaya, K. L. Ivanov, *Mol. Phys.* **2019**, *117*, 2762–2771.
- [10] A. Svyatova, I. V. Skovpin, N. V. Chukanov, K. V. Kovtunov, E. Y. Chekmenev, A. N. Pravdivtsev, J.-B. Hövener, I. V. Koptug, *Chem. – Eur. J.* **2019**, *25*, 8465–8470.
- [11] A. N. Pravdivtsev, K. Buckenmaier, N. Kempf, G. Stevanato, K. Scheffler, J. Engelmann, M. Plaumann, R. Koerber, J.-B. Hövener, T. Theis, *J. Phys. Chem. C* **2023**, *127*, 6744–6753.
- [12] A. B. Schmidt, J. Eills, L. Dagys, M. Gierse, M. Keim, S. Lucas, M. Bock, I. Schwartz, M. Zaitsev, E. Y. Chekmenev, S. Knecht, *J. Phys. Chem. Lett.* **2023**, *14*, 5305–5309.
- [13] J. G. Skinner, G. J. Topping, L. Nagel, I. Heid, C. Hundshammer, M. Grashei, F. H. A. van Heijster, R. Braren, F. Schilling, *Magn. Reson. Med.* **2023**, *90*, 894–909.
- [14] A. B. Schmidt, S. Berner, M. Braig, M. Zimmermann, J. Hennig, D. von Elverfeldt, J.-B. Hövener, *PLOS ONE* **2018**, *13*, e0200141.
- [15] H. Wolinsky, S. Glagov, *Circ. Res.* **1967**, *20*, 99–111.
- [16] ICH HARMONISED GUIDELINE Q3C(R8), **2021**.
- [17] ICH HARMONISED GUIDELINE Q3D(R2), **2022**.
- [18] S. J. Nelson, J. Kurhanewicz, D. B. Vigneron, P. E. Z. Larson, A. L. Harzstark, M. Ferrone, M. van Criekinge, J. W. Chang, R. Bok, I. Park, G. Reed, L. Carvajal, E. J. Small, P. Munster, V. K. Weinberg, J. H. Ardenkjaer-Larsen, A. P. Chen, R. E. Hurd, L.-I. Odegardstuen, F. J. Robb, J. Tropp, J. A. Murray, *Sci. Transl. Med.* **2013**, *5*, 108.

## Author Contributions

Investigation: HdM, PG, OM, MW, LN, MH, ZW, RW, LH, WR, SK, ABS. Data curation: HdM, PG, OM, LN, LH, ABS. Funding acquisition: WR, TR, HJ, RZ, MB, DvE, MZ, SG, JBH, EYC, FS, SK, ABS. Conceptualization: SG, SK, ABS. Methodology: HdM, PG, OM, MW, LH, SeK, SG, SK, ABS. Resources: TR, HJ, MB, DvE, MZ, SK, ABS. Supervision: TR, HJ, MB, DvE, MZ, FS, SK, ABS. Visualization: HdM, PG, OM, LN, MP, JBH, SK, ABS. Discussion of results: all authors. Writing original draft: SG, JBH, EYC, SK, ABS. Review & editing: all authors.